Selective Electrocatalytic Activity of Ligand Stabilized Copper Oxide Nanoparticles

Douglas R. Kauffman,[*,†] *Paul R. Ohodnicki,*[†] *Brian W. Kail,*[‡,†] *Christopher Matranga*[†]

[†]National Energy Technology Laboratory (NETL), United States Department of Energy, 626 Cochrans Mill Road, Pittsburgh, Pennsylvania 15236

[‡]URS, P.O. BOX 618, South Park, Pennsylvania 15219

AUTHOR EMAIL ADDRESS: Douglas.Kauffman@UC.NETL.DOE.GOV

RECEIVED DATE

ABSTRACT. Ligand stabilization can influence the surface chemistry of Cu oxide nanoparticles (NPs) and provide unique product distributions for electrocatalytic methanol (MeOH) oxidation and CO_2 reduction reactions. Oleic acid (OA) stabilized Cu_2O and CuO NPs promote the MeOH oxidation reaction with 88% and 99.97% selective HCOH formation, respectively. Alternatively, CO_2 is the only reaction product detected for bulk Cu oxides and Cu oxide NPs with no ligands or weakly interacting ligands. We also demonstrate that OA stabilized Cu oxide NPs can reduce CO_2 into CO with a ~1.7-fold increase in CO / H_2 production ratios compared to bulk Cu oxides. The OA stabilized Cu oxide NPs also show 7.6 and 9.1-fold increases in CO / H_2 production ratios compared to weakly stabilized

and non-stabilized Cu oxide NPs, respectively. Our data illustrates that the presence and type of surface ligand can substantially influence the catalytic product selectivity of Cu oxide NPs.

TOC Graphic

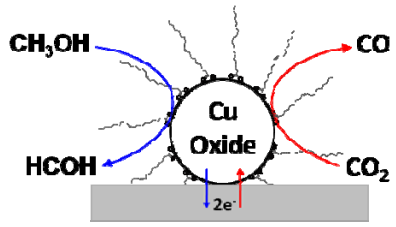

Keywords: nanoparticles, copper oxide, electrocatalysis, methanol oxidation, CO_2 reduction

Organic ligands are commonly used as stabilizing agents during the synthesis of nanoparticles (NPs),[1-3] but little is known about their effect on the NP reactivity. Relative change to a particular catalytic rate is a common metric for describing ligand effects and any changes are typically attributed to surface coverage considerations or control over the NP size.[4-6] A few reports have considered that ligands could play a more active role in dynamic control over NP aggregation,[7] charge transfer with the NP surface,[8,9] influence over support interactions,[10] or control over reactant access to the NP surface.[11] Along these lines, one could also consider a situation where stabilization of particular reactive sites or surface structures may influence both catalytic activity and product selectivity.

Metal oxide NPs are an interesting platform to study ligand influenced electrocatalysis because their surface composition and oxidation state can influence reactivity and product selectivity towards reactions such as methanol (MeOH) oxidation[12] and CO_2 reduction.[13,14] We have used MeOH oxidation as a model reaction to investigate the product selectivity of a variety of bulk and nanoparticulate copper oxides. Oleic acid (OA) stabilized Cu oxide NPs promote the highly selective formation of HCOH,

whereas CO_2 was the only reaction product detected for bulk Cu oxides and Cu oxide NPs with no ligands or weakly interacting ligands. While the six-electron oxidation of MeOH into CO_2 is an important reaction for fuel cell applications,[15] our observation of highly selective HCOH formation is an interesting demonstration of ligand influenced surface chemistry. Moreover, selective HCOH formation has practical applications because annual HCOH consumption exceeds 25 million tons.[16]

In addition to MeOH oxidation, the electrochemical reduction of CO_2 has also been used to investigate the influence of ligands on Cu oxide NP reactivity and selectivity. The conversion of CO_2 into value added products has positive implications in carbon management technologies[17,18] and could serve as an important resource for the production of industrial chemicals.[19,20] Additionally, CO_2 reduction at Cu electrodes is an interesting reaction to study because the nature of active sites and role of surface oxides is still under debate.[13,14] We find that OA stabilized Cu oxide NPs convert CO_2 into CO with reduced H_2 evolution compared to bulk Cu oxides and Cu oxide NPs with no ligands or weakly interacting ligands. Specifically, OA stabilized Cu oxide NPs improve CO / H_2 production ratios by factors of ~1.7 compared to bulk Cu oxides and by factors of 7.6 and 9.1 compared to weakly or non-stabilized Cu oxide NPs, respectively. Our data indicates that OA ligands influence product selectivity for both the MeOH oxidation and CO_2 reduction reactions by sustaining reactive sites on the NP surface during the application of anodic or cathodic electrochemical potentials.

Pt-based electrocatalysts are the state-of-the-art material for MeOH oxidation applications because they demonstrate high catalytic activities and low onset potentials.[15] However, the high cost of Pt-based materials has motivated ongoing research into the use of alternative metals.[12,21-24] Electron microscopy and Raman spectroscopy of OA stabilized Cu oxide NPs (OA-Cu_2O and OA-CuO) are presented in Figure 1, and X-ray photoelectron spectroscopy provides stoichiometric Cu/O atomic ratios that corroborate the Raman-based oxidation state assignments (Fig. S2). FTIR absorbance spectroscopy indicates that OA is attached to the NP surface in a bidentate configuration *via* covalent O–Cu bonds (Fig. S3),[25] and Scherrer equation calculations from X-ray diffraction patterns provide NP sizes within the standard deviation of those estimated from electron microscopy (Fig. S4). Bulk Cu oxide samples

contained particles ranging from 2 μm to 50 μm as determined by scanning electron microscopy. The Cu oxide samples were dispersed in a 1:1 mass ratio with Vulcan XC-72R carbon black (CB) for electrochemical experiments, and cyclic voltammetry (CV) indicated that the NP surfaces were electrochemically accessible in a variety of aqueous solutions (Figs. S5–S7).

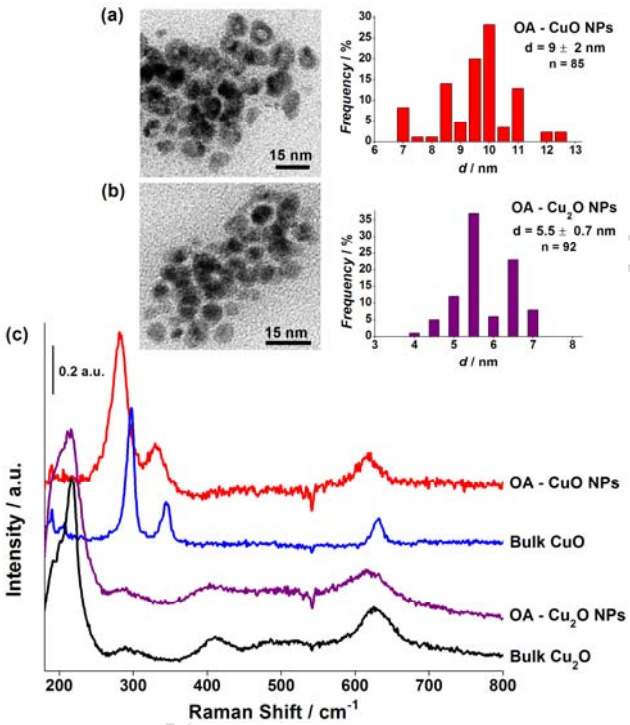

Figure 1. Representative scanning transmission electron microscope images and particle size distributions of the oleic acid (OA) stabilized (a) CuO and (b) Cu_2O nanoparticles (NPs) (c) Raman scattering spectra of bulk Cu oxides and OA stabilized Cu oxide NPs; the spectra are scaled and offset to emphasize peak positions, and peak assignments can be found in Figure S1 in the Supporting Information.

Alkaline electrolytes are a convenient medium to study MeOH oxidation because they typically demonstrate lower onset potentials than acidic solutions,[15] allowing one to study this reaction on a wide variety of catalyst materials. Figure 2a presents CVs of OA-CuO NPs in the absence and presence of MeOH plotted as a function of mass normalized current (mass activity, j_m) where MeOH oxidation

proceeds with diffusion limited behavior (inset Fig. 2a).[26] Figure 2b shows MeOH oxidation curves for OA-stabilized Cu oxide NPs, bulk Cu oxides, bulk Cu foil and CB support. OA-CuO NPs show the highest mass activity and least anodic onset potential of all the catalyst materials considered, and similar results are found when the current is normalized to the electrochemical surface area (ECSA) of each catalyst (Fig. S8). In comparison, literature reports show that ligand stabilized Au NPs can oxidize MeOH at less anodic potentials (~1.3 V *vs*. RHE), but with smaller mass activity (~20 mA mg^{-1}) or current density (~0.170 mA cm^{-2}).[27,28]

Each catalyst was held at a potential of 1.9 V for 1 hour in N_2 saturated 0.1 M NaOH + 1M MeOH in a sealed two compartment H-type cell and the products were analyzed using gas chromatography (GC). We found that bulk Cu foil produces CO_2 ($7.76 \pm 0.02 \times 10^{-4}$ mmol g^{-1} hr^{-1}) and small amounts of CO and H_2 ($3.6 \pm 0.3 \times 10^{-6}$ and $3.2 \pm 0.7 \times 10^{-5}$ mmol g^{-1} hr^{-1}, respectively). CO_2 was the only detected MeOH oxidation product for the bulk Cu oxides with current efficiencies (CEs) ranging between 22% – 37%. On the other hand, OA-Cu_2O NPs and OA-CuO NPs oxidize MeOH into HCOH with 88% and 99.97% selectivity, respectively, and CEs ranging between 87% – 103%. The catalyst free CB support did not produce any detectable reaction products. Figure 2c and Table S1 summarize the measured product formation rates.

MeOH oxidation experiments were also conducted with 22 ± 6 nm poly(vinylpyrrolidone) (PVP)-stabilized Cu_2O NPs[29] and 5 ± 2 nm non-ligand stabilized CuO NPs[30] to evaluate how the presence of weakly interacting ligands or the complete absence of ligand molecules impacts selectivity (Fig. S9). PVP-Cu_2O NPs were chosen for evaluation because PVP is known to interact weakly with the surface of Cu oxide NPs and the synthetic methods are well established.[29] PVP stabilized CuO NPs are not easily produced so we evaluated non-stabilized CuO NPs that were synthesized by a quick precipitation method.[30] The PVP-Cu_2O NPs and non-stabilized CuO NPs do not display the product selectivity observed for OA stabilized Cu oxide NPs. In fact, CO_2 was the only MeOH oxidation product found within our detection limits (Table S1).

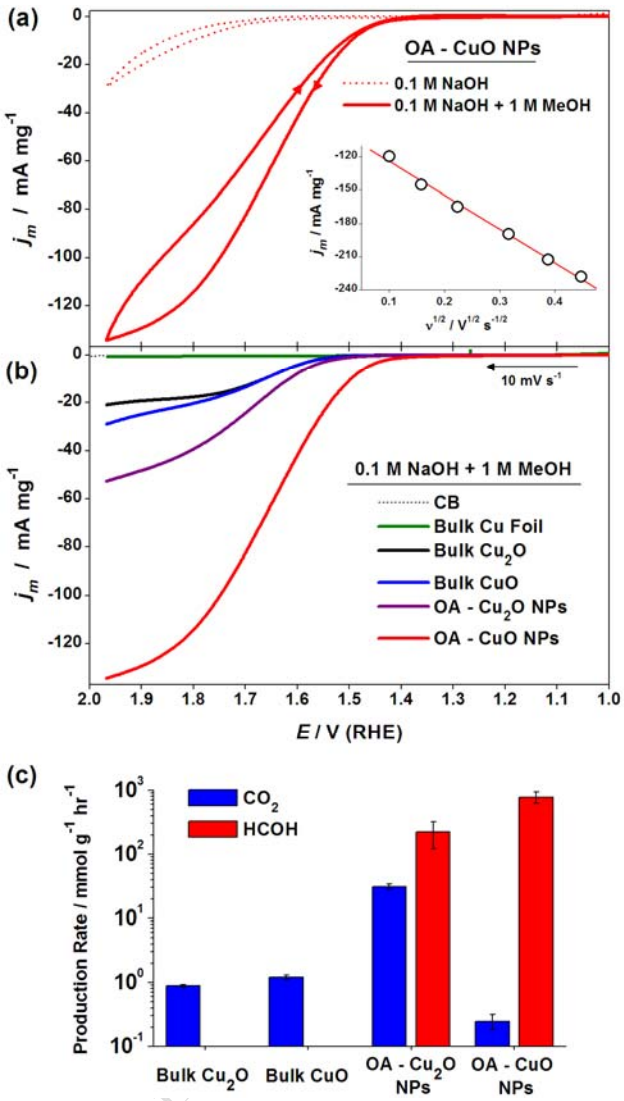

Figure 2. a) Cyclic voltammograms (CVs) of carbon black (CB) supported OA-CuO NPs in the absence (dashed curve) and presence (solid curve) of MeOH; CVs were collected at a scan rate of 10 mV s^{-1}, solutions were N_2 saturated, and the inset shows diffusion limited MeOH oxidation behavior as measured at 1.9 V.[26] b) MeOH oxidation polarization curves for the CB supported Cu oxide materials, bulk Cu foil, and CB support. Qualitatively similar results are found when the current is normalized to the electrochemical surface area (ECSA; Fig. S8). (c) Log_{10} scale plot of the product formation rates after 1 hour of MeOH oxidation at 1.9 V; error bars are from 3 individual runs.

The initial steps in MeOH oxidation at Cu electrodes are generally accepted as OH^- adsorption and formation of a Cu^{3+} containing mixed oxide/hydroxide surface layer.[12] Our data indicates that mixed

oxide/hydroxide layer formation occurs for the bulk Cu oxide materials (Fig. S5) and PVP-Cu_2O NPs (Fig. S9). The non-stabilized CuO NPs show signs of dissolution after repeated cycling through anodic potentials so mixed layer formation cannot be determined unambiguously (Fig. S9). In comparison, mixed oxide/hydroxide layer formation is suppressed at the OA stabilized Cu oxide NPs. Au electrodes are also known to oxidize alcohols into their corresponding aldehydes.[31] However, it is interesting that HCOH was only formed at the OA stabilized NPs because it demonstrates ligand influenced surface chemistry. The selective HCOH production and inhibited mixed oxide/hydroxide layer formation observed for the OA-stabilized NPs, but not the other NP samples, rules out size-related product selectivity. Rather, these results indicate that the oleic acid ligands prevent the formation of a mixed oxide/hydroxide layer, protect the NP from dissolution at anodic potentials, and sustain the reactive sites needed for HCOH formation.

Previous single crystal studies have indicated that partially oxidized Cu surfaces with adjacent O and Cu atoms are required for the thermally activated MeOH → HCOH reaction.[32,33] This particular surface structure promotes MeOH adsorption and HCOH formation *via* interactions between electropositive Cu surface atoms and lone pair electrons in MeOH hydroxyl groups. Ligand exchange[34] or desorption[4] can change the NP surface structure and may affect catalytic activity, but FTIR spectroscopy confirms OA attachment to both the OA-CuO NP and OA-Cu_2O NP surface after 100 MeOH oxidation cycles between 0.0 V and 0.9 V (Fig. S10). This result indicates the retention of covalent O–Cu surface bonds during the electrocatalytic reaction, and we hypothesize that OA promotes HCOH formation by sustaining reactive sites similar to those required for the thermal MeOH → HCOH process. Because ligand interactions are restricted to surface atoms,[35] the two NP systems could have similar Cu and O atom surface sites without significantly impacting their overall Cu/O stoichiometry. The stabilization of adjacent Cu and O surface atoms helps explain the enhanced HCOH production observed for the OA-Cu_2O and OA-CuO NPs, as well as the absence of this product for the bulk materials, non-stabilized CuO NPs, and PVP-Cu_2O NPs.

We have also investigated the role that ligands play in the CO_2 reduction reaction. The use of Cu electrodes to reduce CO_2 in aqueous systems has been studied previously,[13,14] yet competitive H_2 evolution remains a barrier for advancing this technology and specifics concerning the active sites and reaction mechanisms are still debated. Others have reported CO_2 reduction at oxidized Cu foils,[36-39] Zn supported Cu oxide particles (~33−100 nm),[40] and carbon supported submicron Cu_2O cubes,[41] but the role of the oxide remains unclear. In fact, the presence of oxides on Cu electrodes has been suggested by various authors to either inhibit the adsorption of poisoning species,[36] prevent the protonation of adsorbed CO,[37] or facilitate intermediate protonation by providing CO_2 and proton adsorption/reaction sites.[38-40]

Figure 3a presents polarization curves for OA-CuO NPs in N_2 (pH = 9.1) and CO_2 (pH = 7.2) saturated 0.1M $KHCO_3$. In N_2 saturated solution, OA-CuO NPs retain a $Cu^{+/0}$ reduction peak after repeated cycling (20 scans), which we interpret as the retention of some fraction of the surface oxide groups despite the cathodic potential window. After saturating the solution with CO_2, OA-CuO NPs experience a decrease in mass activity over the entire potential window and severe attenuation of the $Cu^{+/0}$ redox feature. Decreased mass activity in CO_2 saturated solutions is a well documented characteristic of Cu materials (Fig. S11),[13,14] and the attenuated $Cu^{+/0}$ redox peak indicates that the adsorption and reduction of CO_2 occurs preferentially over the reduction of surface oxide groups. The observed CO_2 reduction onset potential of approximately –0.6 V (*vs*. RHE) is in agreement with previously reported values for Cu-based electrodes in 0.1 M $KHCO_3$ at pH ~7.[13,14] Figure 3b presents stabilized CO_2 reduction curves for the OA stabilized Cu oxide NPs, bulk Cu oxides, CB support, and bulk Cu foil; qualitatively similar results are obtained with the ECSA normalized current (Fig. S8). Figure S9 contains CO_2 reduction curves for PVP-Cu_2O NPs and non-stabilized CuO NPs.

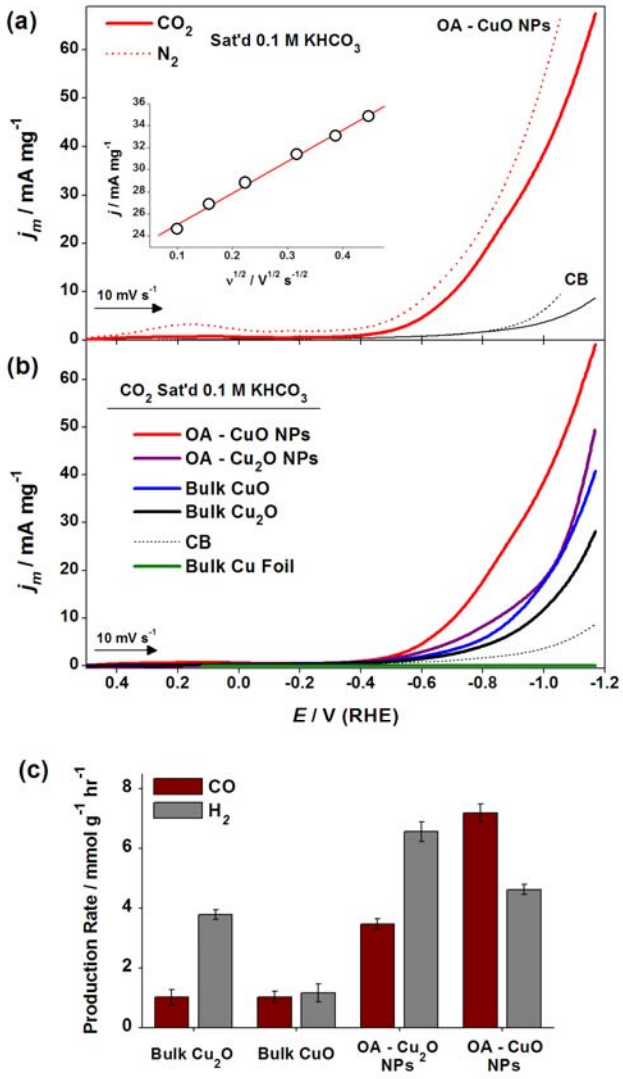

Figure 3. (a) Polarization curves of the CB supported OA-CuO NPs and CB support in N_2 (dashed curve) and CO_2 (solid curve) saturated 0.1 M $KHCO_3$; the inset shows diffusion limited CO_2 reduction behavior as measured at –0.9 V,[26] and an expanded view of the $Cu^{+/0}$ redox feature is shown in Figure S11. (b) CO_2 reduction polarization curves for CB supported Cu oxide materials, bulk Cu foil, and CB support; similar results are found when the current was normalized to the ECSA (Fig. S8). (c) Product formation rates after 1 hour of CO_2 reduction at –0.9 V; error bars are from 3 individual runs.

Each catalyst was held at a potential of –0.9 V (*vs*. RHE) for 1 hour in CO_2 saturated 0.1M $KHCO_3$ in a sealed two compartment H-type cell and reaction products were analyzed by GC, mass spectrometry and ion chromatography. Previously reported CO_2 reduction products can vary depending on

experimental conditions, but HCOOH, H_2 and CO are commonly observed species. In our specific case we find that the bulk Cu foil reproducibly forms HCOOH, H_2 and CO at 0.03 ± 0.01, $9.5 \pm 0.1\times10^{-3}$ and $3.8 \pm 0.6\times10^{-4}$ mmol g^{-1} hr^{-1}, respectively, which is within the range of values previously reported by Hori and others.[13,14] The Cu oxide materials, as a whole, are more selective, with CO and H_2 being the only reaction products detected (Fig. 3c and Table S1). The overall CO and H_2 formation rates for the bulk Cu oxides are comparable to previous experiments conducted at similar potentials in $KHCO_3$.[14] Likewise, CO and H_2 are the only products observed for PVP-Cu_2O NPs and non-stabilized CuO NPs (Table S1). In the absence of a catalyst (only CB support), mostly H_2 (7.3 ± 0.5 mmol g^{-1} hr^{-1}) and smaller amounts of CO (0.33 ± 0.09 mmol g^{-1} hr^{-1}) are found as CO_2 reduction products, and the product formation rates reported in Figure 3c and Table S1 are corrected for the CB support. CEs for the Cu oxides are approximately 3-5%, signifying competitive reduction of some fraction of the catalyst surface.

We have used the ratio of CO and H_2 production rates as a performance metric to quantify catalytic activity and product selectivity (Table S1). OA-Cu_2O NPs and OA-CuO NPs both demonstrate a ~1.7-fold increase in CO / H_2 production ratios over bulk materials and 7.6 and 9.1-fold increases over PVP-Cu_2O NPs and non-stabilized CuO NPs, respectively. Overall, the highest CO formation selectivity is shown by the OA-CuO NPs at 61%, with a balance of 39% H_2. In comparison,[40] non-ligand stabilized, Zn supported Cu oxide particles (33-100 nm) are reported to produce CH_4 and C_2H_4 at 5–7 % selectivity, along with H_2, CO and HCOOH at ~25% selectivity, although direct comparison to our system is difficult due to different reaction conditions.

CO formation is thought to be one of the first steps in the electrochemical reduction of CO_2,[13,14] and the reduction of CO_2 at Cu oxide electrodes has been suggested to proceed at sites containing adjacent Cu and O surface sites.[38,40] This specific surface structure is thought to promote CO_2 reduction by providing adsorption sites for CO_2 and protons, and Hori and coworkers suggest that strong adsorption of $CO_2^{\bullet-}$ intermediate species may lead to selective CO formation.[42] In situ Raman spectroscopy indicates the OA-CuO NPs retain some fraction of surface oxide groups during the application of –0.9 V

in CO_2 saturated 0.1 M $KHCO_3$ (Fig. S12). This behavior is not observed for the bulk Cu oxides, non-ligand stabilized CuO NPs or PVP-Cu_2O NPs, strongly suggesting the OA ligands sustain surface oxide groups on the OA-CuO NP surface. FTIR spectroscopy confirms OA attachment to the OA-CuO NP surface in a bidentate configuration after 100 CO_2 reduction cycles between 0.6 V and −1.2 V (Fig. S10), which further indicates retention of O–Cu surface bonds during CO_2 reduction. The higher CO_2 → CO selectivity of OA-CuO NPs likely occurs because the OA ligands sustain reactive surface oxide sites that promote CO_2 adsorption and conversion into CO. In situ Raman results are less conclusive for the OA-Cu_2O NPs (Fig. S12), but FTIR absorbance spectroscopy indicates retention of covalent O–Cu bonds between the NP surface and OA ligand during the CO_2 reduction reaction (Fig. S10). The improved CO / H_2 selectivity over bulk Cu_2O and PVP-Cu_2O NPs suggests the OA ligands may also stabilize surface sites on the Cu_2O NP to promote CO_2 reduction. The very low CO / H_2 selectivity of the PVP-Cu_2O NPs indicates the coordinative interaction between PVP and the NP surface[29] is too weak to sustain CO forming reactive sites.

In summary, our experimental results demonstrate ligand influenced electrocatalysis where oleic acid ligands promote MeOH oxidation and CO_2 reduction product selectivity. This alludes to better control over product distribution through variation of ligand head groups, their binding configuration and/or surface coverage.

ACKNOWLEDGMENT. D. R. K acknowledges a National Research Council associateship, and the authors thank Dr. J. Baltrus (NETL) for access to and technical assistance with XPS instrumentation. This technical effort was performed in support of the NETL's ongoing research in CO_2 utilization under RES contract DE-FE0004000. Reference in this work to any specific commercial product is to facilitate understanding and does not necessarily imply endorsement by the United States Department of Energy.

SUPPORTING INFORMATION. Experimental details, physical characterization, additional experimental results and discussion. This material is available free of charge via the Internet at http://pubs.acs.org.

REFERENCES

(1) Xia, Y.; Xiong, Y.; Lim, B.; Skrabalak, S. E. Shape-Controlled Synthesis of Metal Nanocrystals: Simple Chemistry Meets Complex Physics? *Angew. Chem. Int. Ed.* **2009**, *48*, 60-103.

(2) Kwon, S. G.; Hyeon, T. Colloidal Chemical Synthesis and Formation Kinetics of Uniformly Sized Nanocrystals of Metals, Oxides, and Chalcogenides. *Acc. Chem. Res.* **2008**, *41*, 1696-1709.

(3) Tao, A. R.; Habas, S.; Yang, P. Shape Control of Colloidal Metal Nanocrystals. *Small* **2008**, *4*, 310-325.

(4) Stowell, C. A.; Korgel, B. A. Iridium Nanocrystal Synthesis and Surface Coating-Dependent Catalytic Activity. *Nano Lett.* **2005**, *5*, 1203-1207.

(5) Li, Y.; El-Sayed, M. A. The Effect of Stabilizers on the Catalytic Activity and Stability of Pd Colloidal Nanoparticles in the Suzuki Reactions in Aqueous Solution. *J. Phys. Chem. B* **2001**, *105*, 8938-8943.

(6) Kuhn, J. N.; Huang, W.; Tsung, C. –K.; Zhang, Y.; Somorjai, G. A. Structure Sensitivity of Carbon−Nitrogen Ring Opening: Impact of Platinum Particle Size from below 1 to 5 nm upon Pyrrole Hydrogenation Product Selectivity over Monodisperse Platinum Nanoparticles Loaded onto Mesoporous Silica. *J. Am. Chem. Soc.* **2008**, *130*, 14026-14027.

(7) Wei, Y.; Han, S.; Kim, J.; Soh, S.; Grzybowski, B. A. Photoswitchable Catalysis Mediated by Dynamic Aggregation of Nanoparticles. *J. Am. Chem. Soc.* **2010**, *132*, 11018-11020.

(8) Zhang, G. –R.; Xu, B. –Q. Surprisingly Strong Effect of Stabilizer on the Properties of Au Nanoparticles and Pt^Au Nanostructures in Electrocatalysis. *Nanoscale* **2010**, *2*, 2798-2804.

(9) Tsunoyama, H.; Ichikuni, N.; Sakurai, H.; Tsukuda, T. Effect of Electronic Structures of Au Clusters Stabilized by Poly(N-vinyl-2-pyrrolidone) on Aerobic Oxidation Catalysis. *J. Am. Chem. Soc.* **2009**, *131*, 7086-7093.

(10) Sonström, P.; Arndt, D.; Wang, X.; Zielasek, V.; Bäumer, M. Ligand Capping of Colloidally Synthesized Nanoparticles—A Way to Tune Metal–Support Interactions in Heterogeneous Gas-Phase Catalysis. *Angew. Chem. Int. Ed.* **2011**, *50*, 3888-3891.

(11) Genorio, B.; Subbaraman, R.; Strmcnik, D.; Tripkovic, D. Tailoring the Selectivity and Stability of Chemically Modified Platinum Nanocatalysts to Design Highly Durable Anodes for PEM Fuel Cells. *Angew. Chem. Int. Ed.* **2011**, *50*, 5468-5472.

(12) Fleischmann, M.; Korinek, K.; Pletcher, D. The Kinetics and Mechanism of the Oxidation of Amines and Alcohols at Oxide-Covered Nickel, Silver, Copper and Cobalt Electrodes. *J. Chem. Soc. Perkin Trans. 2* **1972**, *2*, 1396-1403.

(13) Hori, Y. Electrochemical CO_2 Reduction on Metal Electrodes. *Modern Aspects of Electrochemistry*; Vayenas, C. G.; White, R. E.; Gamboa-Aldeco, M. E.; Eds. Springer, New York, **2008**, *42*, 89-189.

(14) Gattrell, M.; Gupta, N.; Co, A. A Review of the Aqueous Reduction of CO_2 to Hydrocarbons at Copper. *J. Electroanal. Chem.* **2006**, *594*, 1-19.

(15) Cohen, J. L.; Volpe, D. J.; Abruña, H. D. Electrochemical Determination of Activation Energies for Methanol Oxidation on Polycrystalline Platinum in Acidic and Alkaline Electrolytes. *Phys. Chem. Chem. Phys* **2007**, *9*, 49-77.

(16) Qian, M.; Liauw, M. A.; Emig, G. Formaldehyde Synthesis from Methanol Over Silver Catalysts. *Appl. Catal. A* **2003**, *238*, 211-222.

(17) Lacis, A. A.; Schmidt, G. A.; Rind, D.; Ruedy, R. A. Atmospheric CO_2: Principal Control Knob Governing Earth's Temperature. *Science* **2010**, *330*, 356-359.

(18) Davis, S. J.; Caldeira, K.; Matthews, H. D. Future CO_2 Emissions and Climate Change from Existing Energy Infrastructure. *Science* **2010**, *329*, 1330-1333.

(19) Whipple, D. T.; Kenis, P. J. A. Prospects of CO_2 Utilization via Direct Heterogeneous Electrochemical Reduction. *J. Phys. Chem. Lett.* **2010**, *1*, 3451-3458.

(20) D'Alessandro, D. M.; Smit, B.; Long, J. R. Carbon Dioxide Capture: Prospoects for New Materials. *Angew. Chem. Int. Ed.* **2010**, *49*, 6058-6082.

(21) Heli, H.; Jafarian, M.; Mahjani, M. G.; Gobal, F. Electro-Oxidation of Methanol on Copper in Alkaline Solution. *Electrochim. Acta* **2004**, *49*, 4999-5006.

(22) Nagasharee, K. L.; Ahmed, M. F. Electrocatalytic Oxidation of Methanol on Cu Modified Polyaniline Electrode in Alkaline Medium. *J. Appl. Electrochem.* **2009**, *39*, 403-410.

(23) Ferrin, P.; Mavrikakis, M. Structure Sensitivity of Methanol Electrooxidation on Transition Metals. *J. Am. Chem. Soc.* **2009**, *131*, 14381-14389.

(24) Tehrani, R. M. A.; Ab Ghani, S. The Nanocrystalline Nickel with Catalytic Properties on Methanol Oxidation in Alkaline Medium. *Fuel Cells* **2009**, *9*, 579-587.

(25) Wu, N.; Fu, L.; Su, M.; Aslam, M.; Wong, K. C.; Dravid, V. P. Interaction of Fatty Acid Monolayers with Cobalt Nanoparticles. *Nano Lett.* **2004**, *4*, 383-386.

(26) Bard, A. J.; Faulkner, L. R. *Electrochemical Methods: Fundamentals and Applications, 2nd Edition*; John Wiley & Sons: New York, 2001.

(27) Yan, S.; Zhang, S.; Lin, Y.; Liu, G. Electrocatalytic Performance of Gold Nanoparticles Supported on Activated Carbon for Methanol Oxidation on Alkaline Solution. *J. Phys. Chem. C* **2011**, *115*, 6986-6993.

(28) Lou, J.; Jones, V. W.; Maye, M. M.; Han, L.; Kariuki, N. N.; Zong, C. J. Thermal Activation of Molecularly-Wired Gold Nanoparticles on a Substrate as a Catalyst. *J. Am. Chem. Soc.* **2002**, *124*, 13988-13989.

(29) Haas, I.; Shanmugam, S.; Gedanken, A. Pulsed Sonochemical Synthesis of Size-Controlled Copper Nanoparticles Stabilized by Poly(N-vinylpyrrolidone). *J. Phys. Chem. B* **2006**, *110*, 16947-16952.

(30) Zhu, J.; Li, D.; Chen, H.; Yang, X.; Lu, L.; Wang, X. Highly Dispersed CuO Nanoparticles Prepared by a Novel Quick-Precipitation Method. *Mater. Lett.* **2004**, *58*, 3324-3327.

(31) Kwon, Y.; Lai, S. C. S.; Rodriguez, P.; Koper, M. T. M. Electrocatalytic Oxidation of Alcohols on Gold in Alkaline Media: Base or Gold Catalysis? *J. Am. Chem. Soc.* **2011**, *133*, 6914-6917.

(32) Wachs, I. E.; Madix, R. J. The Selective Oxidation of CH_3OH to H_2CO on Copper (110) Catalyst. *J. Catal.* **1978**, *53*, 208-227.

(33) Russell, J. N. Jr.; Gates, S. M.; Yates, J. T. Jr. Reaction of Methanol with Cu(111) and Cu(111) + O(ads). *Surf. Sci.* **1985**, *163*, 516-540.

(34) Liu, Y.; Wang, C.; Wei, Y.; Zhu, L.; Li, D.; Jiang, J. S.; Markovic, N. M.; Stamenkovic, V. R.; Sun, S. Surfactant-Induced Postsynthetic Modulation of Pd Nanoparticle Crystallinity. *Nano Lett.* **2011**, *11*, 1614-1617.

(35) Liu, H.; Gou, J.; Yin, Y.; Augustsson, A.; Dong, C.; Nordgren, J.; Chang, C.; Alivisatos, P.; Thornton, G; Ogletree, D. F.; Requejo, F. G.; de Groot, F.; Salmeron, M. Electronic Structure of Cobalt Nanocrystals Suspended in Liquid *Nano Lett.* **2007**, *7*, 1919-1922.

(36) Lee, J.; Tak, Y. Electrocatalytic Activity of Cu Electrode in Electroreduction of CO_2. *Electrochim. Acta* **2001**, *46*, 3015-3022.

(37) Yano, J.; Yamasaki, S. Pulse-Mode Electrochemical Reduction of Carbon Dioxide Using Copper and Copper Oxide Electrodes for Selective Ethylene Formation. *J. Appl. Electrochem.* **2008**, *38*, 1721-1726.

(38) Le, M.; Ren, M.; Zhang, Z.; Sprunger, P. T.; Kurtz, R. L.; Flake, J. C. Electrochemical Reduction of CO_2 to CH_3OH at Copper Oxide Surfaces. *J. Electrochem. Soc* **2011**, *158*, E45-E49.

(39) Terunuma, Y.; Saitoh, A.; Momose, Y. Relationship Between Hydrocarbon Production in the Electrochemical Reduction of CO_2 and the Characteristics of the Cu Electrode. *J. Electroanal. Chem.* **1997**, *434*, 69-75.

(40) Ohya, S.; Kaneco, S.; Katsumata, H.; Suzuki, T.; Ohta, K. Electrochemical Reduction of CO_2 in Methanol with Aid of CuO and Cu_2O. *Catal. Today* **2009**, *148*, 329-334.

(41) Chang, T. –Y.; Liang, R. –M.; Wu, P. –W.; Chen, J. –Y.; Hsieh, Y. –C. Electrochemical Reduction of CO_2 by Cu_2O-catalyzed Carbon Clothes. *Mater. Lett.* **2009**, *63*, 1001-1003.

(42) Hori, Y.; Wakebe, H.; Tsukamoto, T.; Koga, O. Electrocatalytic Process of CO Selectivity in Electrochemical Reduction of CO_2 at Metal Electrodes in Aqueous Media. *Electrochim. Acta* **1994**, *39*, 1833-1839.

Supporting Information Section

Selective Electrocatalytic Activity of Ligand Stabilized Copper Oxide Nanoparticles

Douglas. R. Kauffman,[*,†] Paul R. Ohodnicki,[†] Brian W. Kail,[†,‡] and Christopher Matranga[†]

† National Energy Technology Laboratory, United States Department of Energy, 626 Cochrans Mill Road, Pittsburgh, Pennsylvania 15236

‡ URS, P.O. Box 618, South Park, Pennsylvania 15219

* Email: Douglas.Kauffman@UC.NETL.DOE.GOV

Contents

Experimental Details (pages S2 – S4).

Fig. S1: Raman spectroscopy peak assignments (page S5).

Fig. S2: Cu 2p region X-ray photoelectron spectroscopy (XPS) (page S6).

Fig. S3: FTIR spectroscopy and XPS of Cu oxide NPs (page S7).

Fig. S4: XRD of Cu-based catalysts (page S8).

Fig. S5: CV of catalysts in N_2 saturated 0.1 M NaOH (page S9).

Fig. S6: CV of Cu oxide catalysts in N_2 saturated 0.1 M $KHCO_3$ (page S10).

Fig. S7: CV of Cu oxide catalysts in N_2 saturated 1.0 M H_2SO_4 (page S11).

Fig. S8: ECSA normalized MeOH oxidation and CO_2 reduction curves (page S12).

Fig. S9: TEM and CV of PVP-stabilized and non-ligand Cu oxide NPs NaOH and $KHCO_3$ (page S13).

Fig. S10.: FTIR spectroscopy of OA stabilized NPs before and after electrocatalytic reactions (page S14).

Fig. S11.: CV of Cu oxide catalysts in N_2 and CO_2 saturated $KHCO_3$ (page S15).

Fig. S12. Raman scattering spectra of catalysts during CO_2 reduction of –1.5 V (page 16)

Table S1: MeOH oxidation and CO_2 reduction product distributions for the Cu oxide catalysts (page S17).

Supporting Information References (pages S18 – S21).

Experimental Details

NP synthesis. Oleic acid (OA) stabilized Cu_2O and CuO nanoparticles (NPs) were synthesized similar to a previously published method.[1] Briefly, Cu (I) acetate (precursor), oleic acid (organic ligand) and trioctylamine (reducing agent) were heated under flowing N_2 past the precursor decomposition temperature to induce NP nucleation and growth. After ~20 minutes at 300^{o}C the mixture became a dark burgundy color, and the reaction was allowed to continue for another 30 minutes until the mixture because very viscous. The different oxidation states were produced by varying the relative amounts of oleic acid and trioctylamine and in the reaction vessel. The particles were purified through repeated sonication/centrifugation cycles in ethanol, and then finally suspended in methanol for future experiments.

Non-ligand stabilized CuO NPs were synthesized by the so called "quick precipitation" method.[2] Specifically, 0.167 μL of glacial acetic acid was added to 50 mL of 0.2 M aqueous Cu(II) acetate and the mixture was refluxed for approximately 30 minutes. Subsequently, 0.133 g of NaOH was dissolved in ~2 mL of H_2O, heated to roughly 80 ^{o}C, and then added very quickly to the refluxing Cu(II) acetate mixture. A dark brown/black precipitate formed immediately after the addition of NaOH, and after cooling to room temperature the precipitate was centrifuged and redispersed several times *via* sonication with H_2O and methanol (MeOH). The final product was dispersed in MeOH for future experiments.

PVP-stabilized Cu_2O NPs were synthesized at room temperature following a method similar to that reported by Schaak and coworkers[3] by mixing 13.6 mg $Cu_2SO_4 \cdot H_2O$ and 120 mg 40,000 MW poly(vinylpyrrolidone) (PVP) in 25 mL H_2O. The solution was briefly sonicated until the PVP was dissolved and purged with N_2 for ~30 min. Under a N_2 atmosphere and with vigorous magnetic stirring, 50 mL 0.1 $NaBH_4$ was slowly introduced dropwise over a period of approximately 2 hours. The resulting NP suspension was rinsed and centrifuged several times with water and the particles were then suspended in MeOH for future experiments.

Physical Characterization. Scanning transmission electron microscopy and scanning electron microscopy were performed on Hitachi S-5500 and FEI Quantum 600F microscopes, respectively. Raman spectra were collected with a Nicolet Almega dispersive Raman spectrometer with a confocal microscope attachment and a 532 nm excitation source. Fourier transform infrared (FTIR) absorption spectra were collected on a Nicolet 7600 spectrometer, and X-ray diffraction (XRD) patterns were collected with on a Phillips MRD Pro Powder diffractometer in a 1^o glancing angle geometry. X-ray photoelectron spectroscopy (XPS) was conducted with a PHI 5600ci spectrometer employing Al Kα X-rays; an electron flood gun was used to neutralize surface charging of the samples,[1] and all XPS binding energies were corrected to the carbon C1s peak at 284.6 eV.

Preparation of Carbon Black-Supported Catalysts. Commercially available bulk Cu_2O (99.9%) and CuO (99.99%) powders (2 μm – 50 μm diameter) and Cu oxide NPs were mixed with commercially available XC-72R carbon black (CB) to a loading of 50% Cu oxide by mass. The Cu oxide and CB were dispersed in MeOH by the addition of a small amount (5% total volume) of commercially available 5% Nafion solution followed by thorough sonication. The

final dispersions contained 0.5 μg/μL of the particular Cu oxide catalyst and 0.5 μg/μL of the CB support.

Electrochemistry. Glassy carbon (GC) electrodes were thoroughly polished with 0.05 μm alumina powder and then sequentially sonicated in methanol and ultrapure deionized water (> 18.0 MΩ). 30 μL of the CB/Cu oxide catalyst dispersion was deposited onto the GC electrode in 10 μL increments and allowed to dry in air. Bulk Cu experiments were performed with a Cu-foil (99.98%) that was scoured with 600 grit sandpaper, rinsed with ultrapure water, and used without any further preparation. Ultrapure deionized water was used to clean all glassware and prepare all electrolyte solutions.

Cyclic voltammetry (CV) and controlled potential electrolysis measurements were performed with a BioLogic SP-150 potentiostat using a Pt-wire counter electrode and a Ag/AgCl (3.0 M NaCl) reference electrode calibrated to the reversible hydrogen electrode (RHE) scale with a commercially available Hydroflex hydrogen reference electrode; $E^0_{(RHE)} = 0.000 - 0.059*pH$.[4] CV studies of the MeOH oxidation and CO_2 reduction reaction were conducted in a standard single-chamber cell in N_2 or CO_2 saturated solutions under a N_2 or CO_2 atmosphere *without* stirring the solution. All reported plots are stabilized unless specified otherwise, ***i.e***. the scans were repeated until no change in the CV was observed (typically 20 scans), and polarization curves presented in the main text were taken from stabilized CVs.

Controlled potential MeOH oxidation reactions were performed in a sealed two-compartment H-type cell separated by a 0.1778 mm (0.007 inch) thick Nafion 117 membrane. The compartment housing the working and reference electrodes contained N_2 saturated 1.0 M MeOH + 0.1 M NaOH and the compartment housing the counter electrode contained N_2 saturated 0.1 M NaOH. A potential of 1.9 V (*vs.* RHE) was applied to the working electrode while a magnetic stirrer prevented the accumulation of bubbles at the electrode surface; a consistent stirring speed was used for all experiments. After applying 1.9 V (*vs.* RHE) for one hour, the products were analyzed using a gas chromatogram (GC) equipped with both FID and TCD detectors. The reported production rates are the average of at least three runs with individually prepared electrodes.

CO_2 reduction reactions were performed in a nearly identical manner as described above, except both compartments of the H-type cell were filled with 0.1M $KHCO_3$. The solution in the working electrode compartment was saturated with CO_2 and the counter electrode compartment solution was saturated with N_2. A voltage of –0.9 V (*vs.* RHE) was applied to the working electrode while a magnetic stirrer prevented the accumulation of bubbles at the electrode surface; a consistent stirring speed was used for all experiments. After applying –0.9 V (*vs.* RHE) for one hour, the products were analyzed using GC, GC coupled to a mass spectrometer and ion chromatography. The reported production rates are the average of at least three runs with individually prepared electrodes.

The electrochemical surface area (ECSA) was estimated from CV in NaOH and $KHCO_3$ (Figs. S5 and S6).[5] In $KHCO_3$ we used the average charge (integrated peak area) associated with both the $Cu^{0/+}$ and $Cu^{+/2+}$ processes, whereas in NaOH only the $Cu^{0/+}$ peak was well defined due to mixed oxide/hydroxide layer formation at more anodic potentials. The charge per one-electron

process divided by Faraday's constant provided the total electrons consumed, which divided by the average areal density of polycrystalline Cu (1.46×10^{15} atoms cm^{-2})[6] provided an estimate for the ECSA. Using this method a charge density of 233 $\mu C/cm^2$ was obtained, which is in reasonable agreement with typical values of 420 $\mu C/cm^2$ and 320 $\mu C/cm^2$ for polycrystalline Pt and Au, respectively.[5] We note here that ECSA determination *via* the $H_{ads/des}$ technique, as is common with Pt-group metals, was not appropriate for our materials due to Cu redox features in the $H_{ads/des}$ regions in acidic solutions (Fig. S7). Unlike Pt-based materials, there is a certain degree of uncertainty in the experimental determination of ECSA for first row transition metals because of the assumption that all redox active sites are located on the surface. Accordingly, we have chosen to present our results with respect to the mass normalized current "j_m" (mass activity), however, we present the ECSA-normalized current, "j_A" (current density) as a comparison in Figure S8.

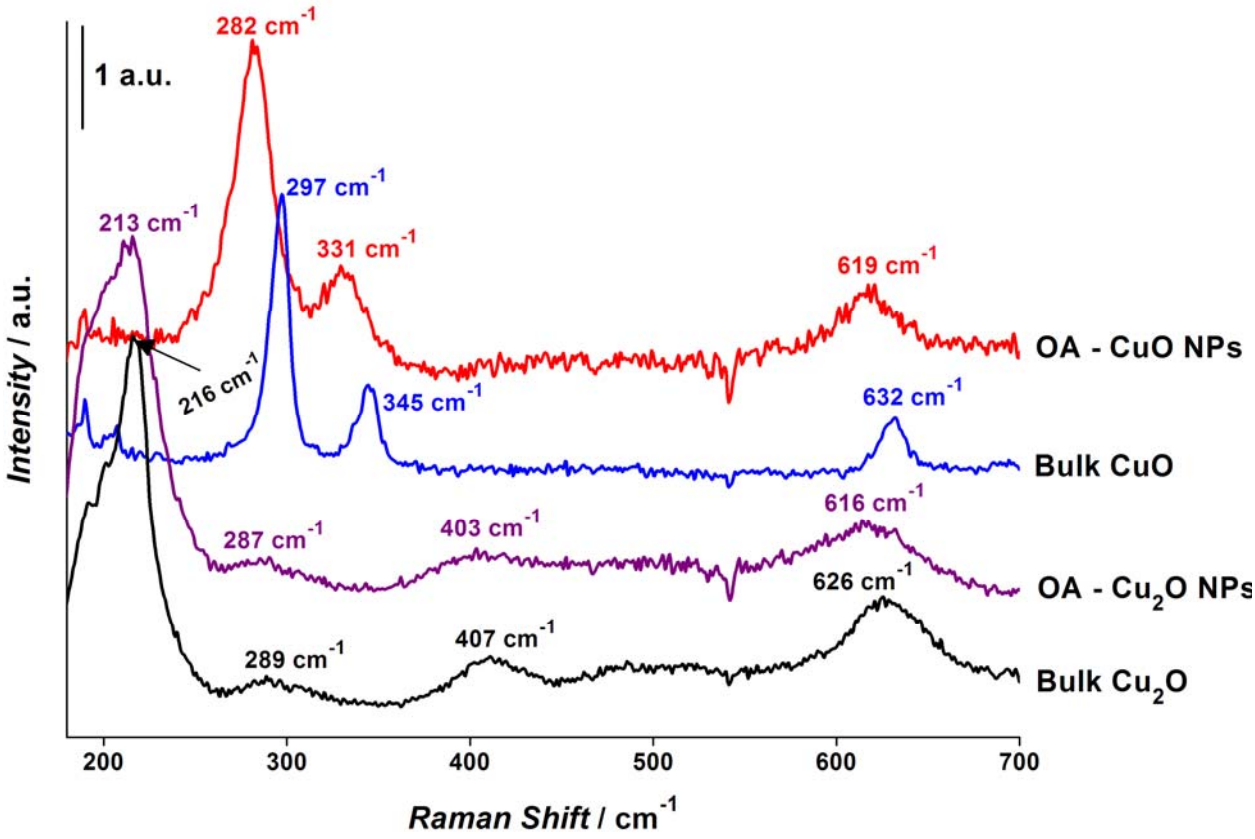

Figure S1. Raman peak assignments for bulk Cu oxides and oleic acid (OA) stabilized Cu oxide NPs; the spectra have been scaled and offset to emphasize peak positions

Bulk CuO and OA-CuO NPs share a similar spectra, with bulk peaks at 632, 345 and 297 cm^{-1} corresponding to the B^2_g, B^1_g and A_g optical modes, respectively.[7] However, the OA-CuO NP peaks are shifted towards lower wavenumbers and somewhat broadened due to their reduced dimensionality.[8] The Cu_2O samples also share similar spectral features with a bulk Cu_2O peak at 626 cm^{-1} corresponding to the F^1_u mode of Cu_2O, two peaks corresponding to multiphonon processes at 500 and 407 cm^{-1}, a peak at ~290 cm^{-1} corresponding to the A^2_u mode, and a peak at ~220 cm^{-1} that contains the $2E_u$ and two fundamental resonance modes.[9] Again, the OA-Cu_2O NP peaks are shifted towards lower wavenumbers and are somewhat broadened as compared to the bulk sample.

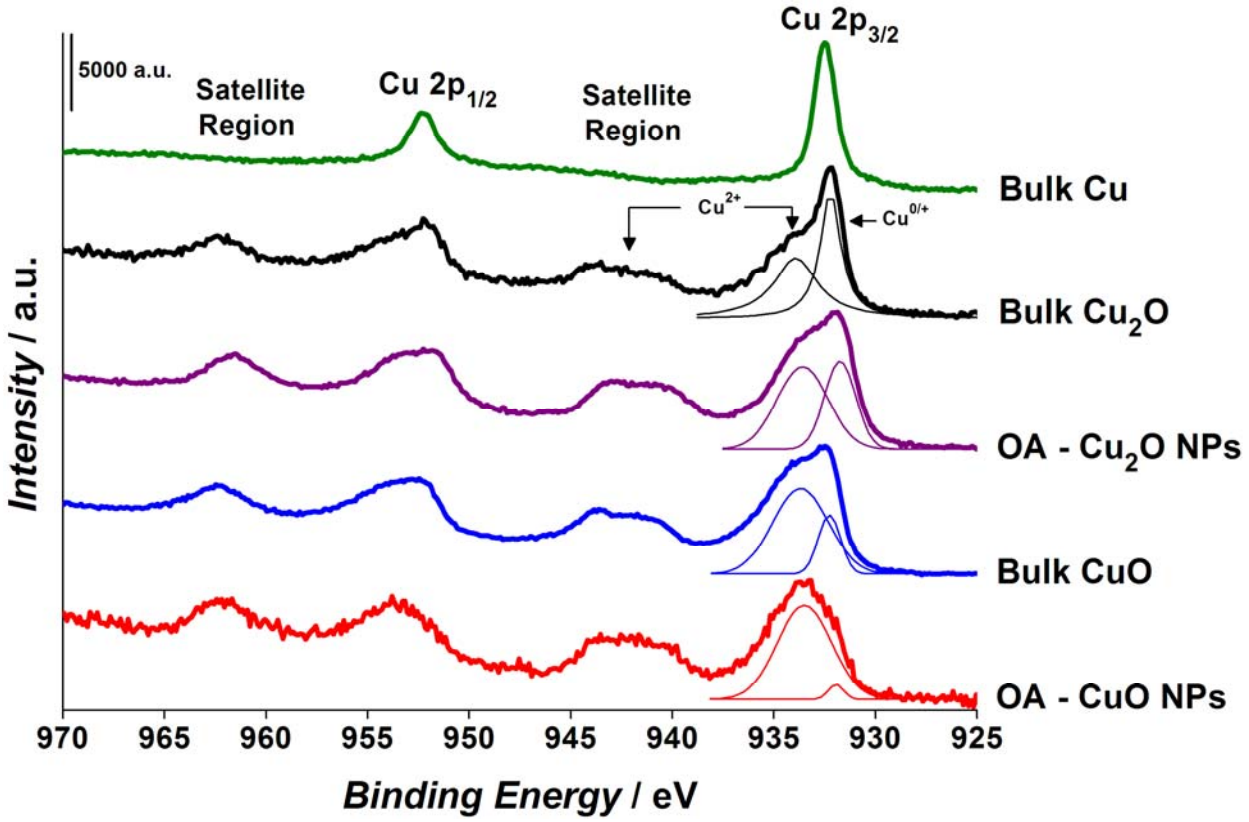

Figure S2. XPS of the Cu 2p region for all of the Cu-based catalysts; the spectra have been scaled and offset to emphasize peak positions.

The feature centered around 932 eV represents the Cu $2p_{3/2}$ region, but spectral overlap between Cu^0 and Cu^+ precludes differentiation with XPS.[10] However, calculated stoichiometric Cu/O atomic ratios, based on the integrated areas of the Cu 2p and O 1s regions,[11] provide a Cu/O ratio of 13 for the bulk Cu foil. The bulk foil Cu $2p_{3/2}$ feature was fit with a single peak assigned to $Cu^{0/+}$.

Cu/O ratios are calculated to be 2.1 for bulk Cu_2O and 1.1 for bulk CuO, yielding stoichiometries consistent with vibrational spectrum for these oxides as determined by Raman spectroscopy (Fig. S1). The Cu $2p_{3/2}$ region of the Cu-oxide samples is fit with two peaks with energy positions corresponding to Cu^{2+} (~933.5 eV) and $Cu^{0/+}$ (~932.0 eV).[10,11] Cu^{2+} peaks in the fitted Cu $2p_{3/2}$ feature and a higher energy satellite[10] were seen in all of the Cu oxide samples. These are typical features of Cu oxides exposed to air and can be attributed to a thin surface layer of CuO.[10,12] The Cu/O ratios were calculated to be 1.5 and 0.82 for the OA-Cu_2O and OA-CuO NPs. The lower Cu/O ratio could be due to the reduced size (increased surface area) of the NPs, or the attachment of the oleic acid ligands to the NP surface *via* O-Cu bonds (see Fig. S3 for further details).

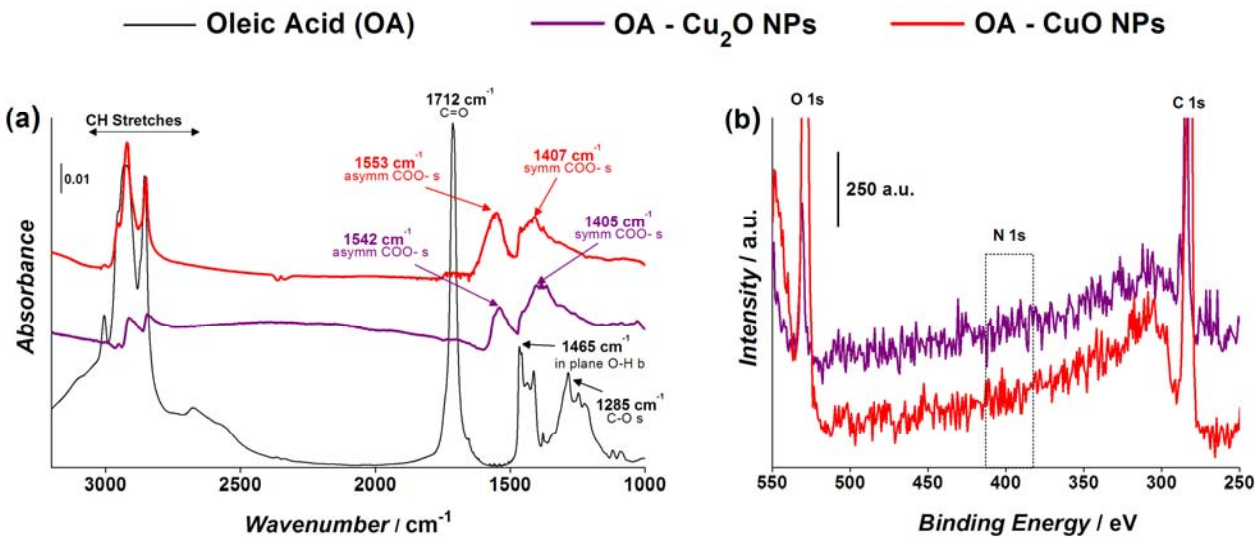

Figure S3. a) FTIR absorbance spectra of oleic acid (OA; black curve), OA-CuO NPs (red curve) and OA-Cu_2O NPs (purple curve). The free oleic acid C=O stretch (1712 cm^{-1}) is split into asymmetric and symmetric COO- stretches when bound to the NP surface in a bidentate O-Cu binding configuration;[13] the spectra have been offset for clarity. b) X-ray photoelectron spectroscopy (XPS) of the OA stabilized Cu oxide NPs highlighting the absence of a peak in the N 1s region; the spectra have been offset for clarity. A lack of detectible N 1s peaks, along with the characteristic oleic acid FTIR bands (panel a), indicate that the NPs are capped with OA ligands and not the reducing agent trioctylamine.

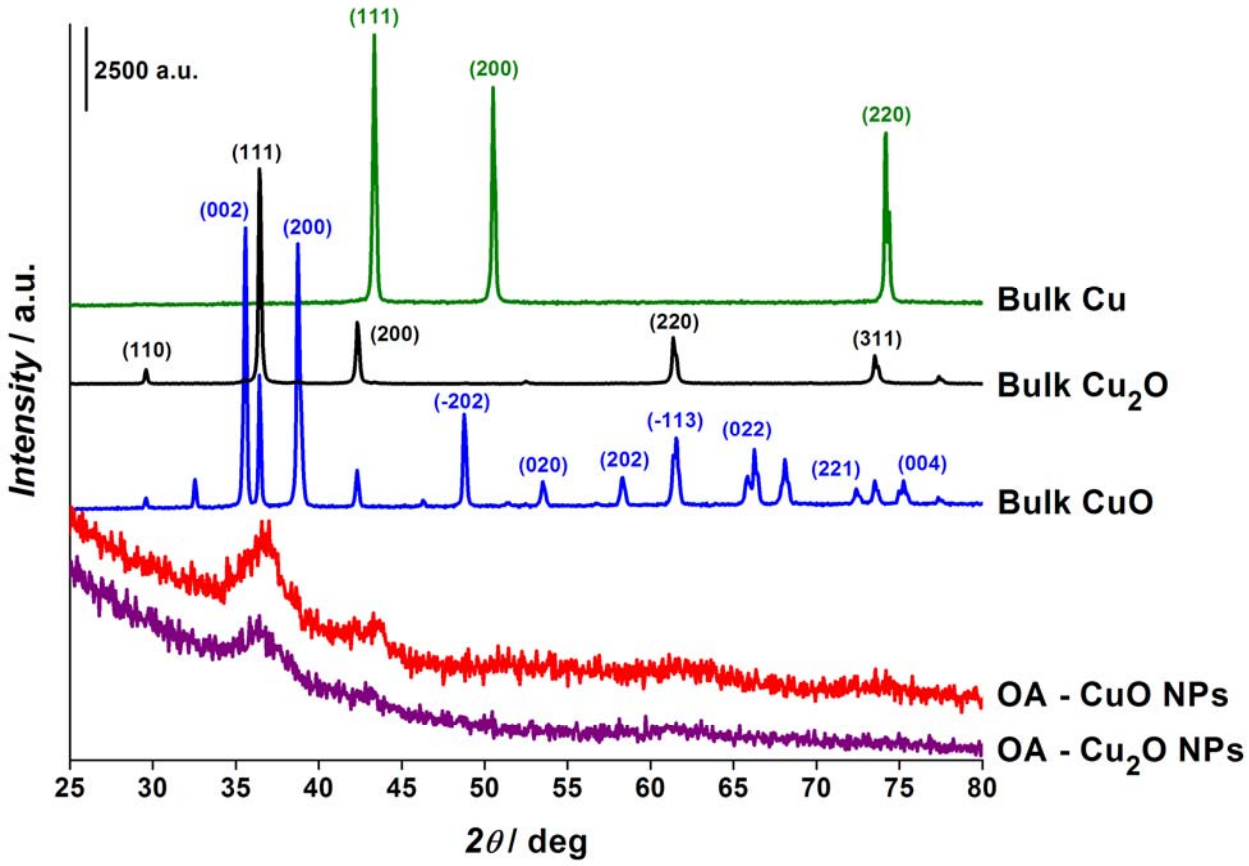

Figure S4. XRD patterns of bulk Cu, bulk Cu oxides and OA stabilized Cu oxide NPs; the curves have been scaled and offset. See supporting information reference 14 for diffraction peak assignments. Scherrer equation calculations based on the peak at approximately 36 degrees provide sizes of 7 nm for OA-CuO NPs and 5 nm for the OA-Cu_2O NPs. These calculated values fall within the standard deviations of those estimated from electron microscopy (9 ± 2 nm for OA-CuO NPs and 5.5 ± 0.7 nm for OA-Cu_2O NPs), as presented in Figure 1 of the main text.

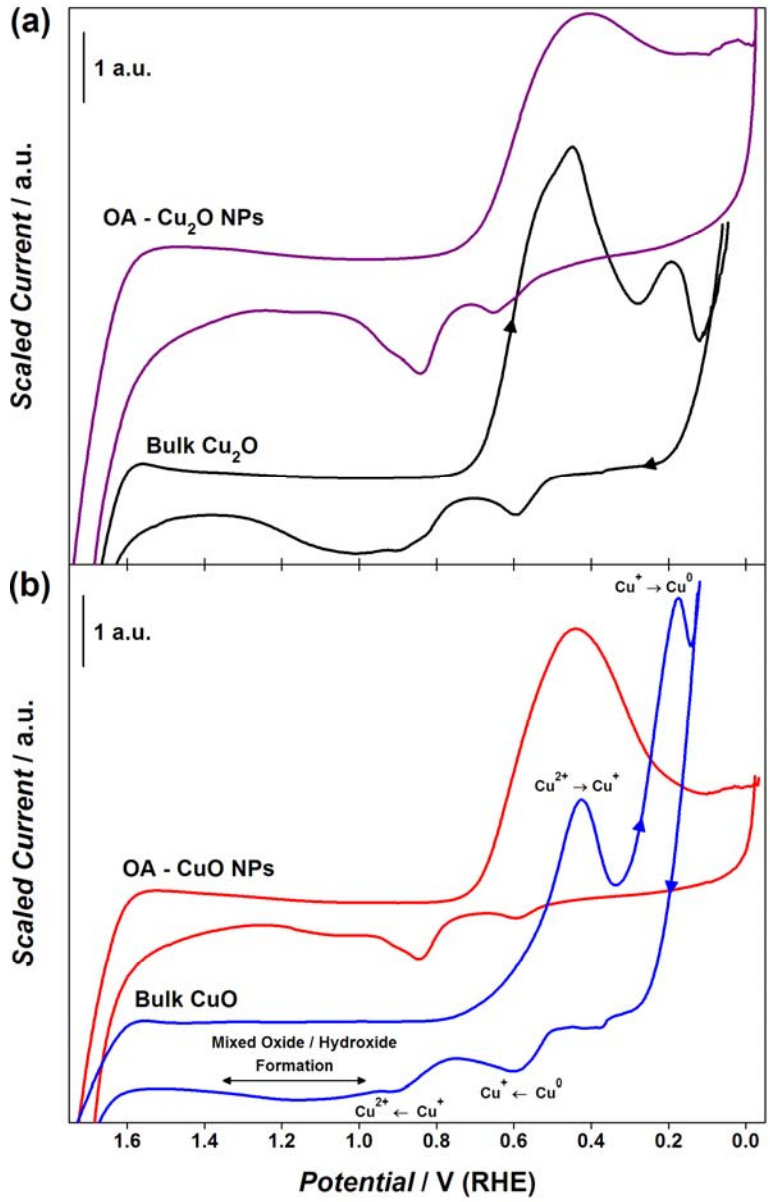

Figure S5. Stabilized CVs of CB-supported Cu oxide materials in N_2 saturated 0.1 M NaOH; curves have been scaled and offset for clarity. The corresponding redox processes have been labeled for the bulk CuO curve in panel b, the scan direction is indicated with arrows, and a scan rate of 10 mV s^{-1} was used for all curves.

In N_2 saturated 0.1 M NaOH a feature between ~0.9 V and 1.4 V (*vs*. RHE) corresponds to the formation of a mixed oxide/hydroxide layer on the bulk Cu oxides.[15] This process was severely attenuated for the OA stabilized Cu oxide NPs, indicating that the formation of a mixed oxide/hydroxide layer was suppressed by the OA ligands attached to the NP surface.

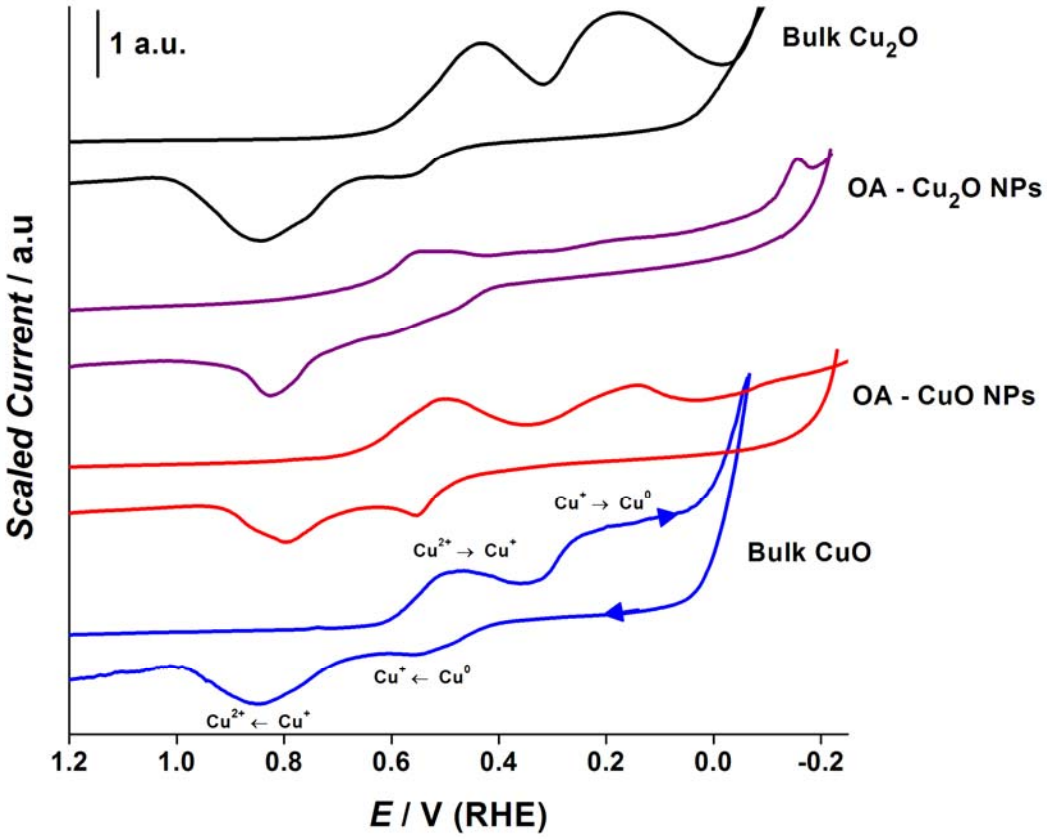

Figure S6. Stabilized CVs of CB-supported Cu oxides in N_2 saturated 0.1 M $KCHO_3$; the curves have been scaled and offset for clarity. The corresponding redox processes have been labeled on the bulk CuO curve, the scan direction is indicated with arrows, and a scan rate of 10 mV s^{-1} was used for all curves.

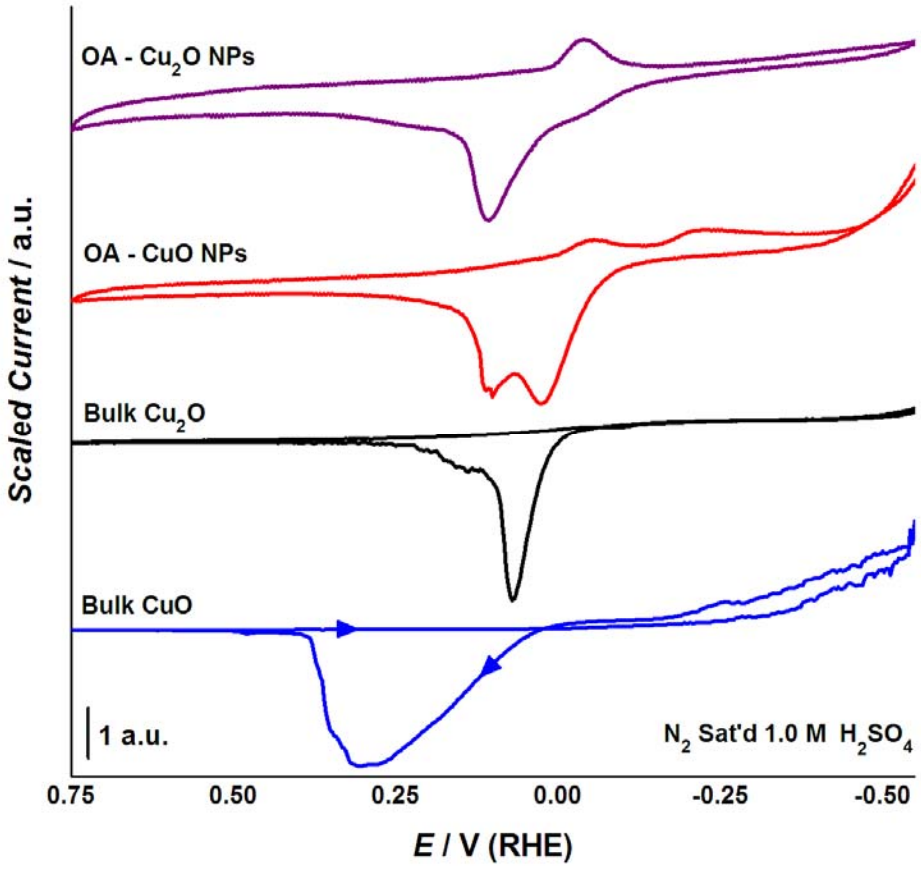

Figure S7. Stabilized CVs of CB-supported Cu oxides in N_2 saturated 1.0 M H_2SO_4; currents have been scaled and offset, the scan direction is indicated with arrows on the bulk CuO curve, and a scan rate of 10 mV s^{-1} was used for all curves.

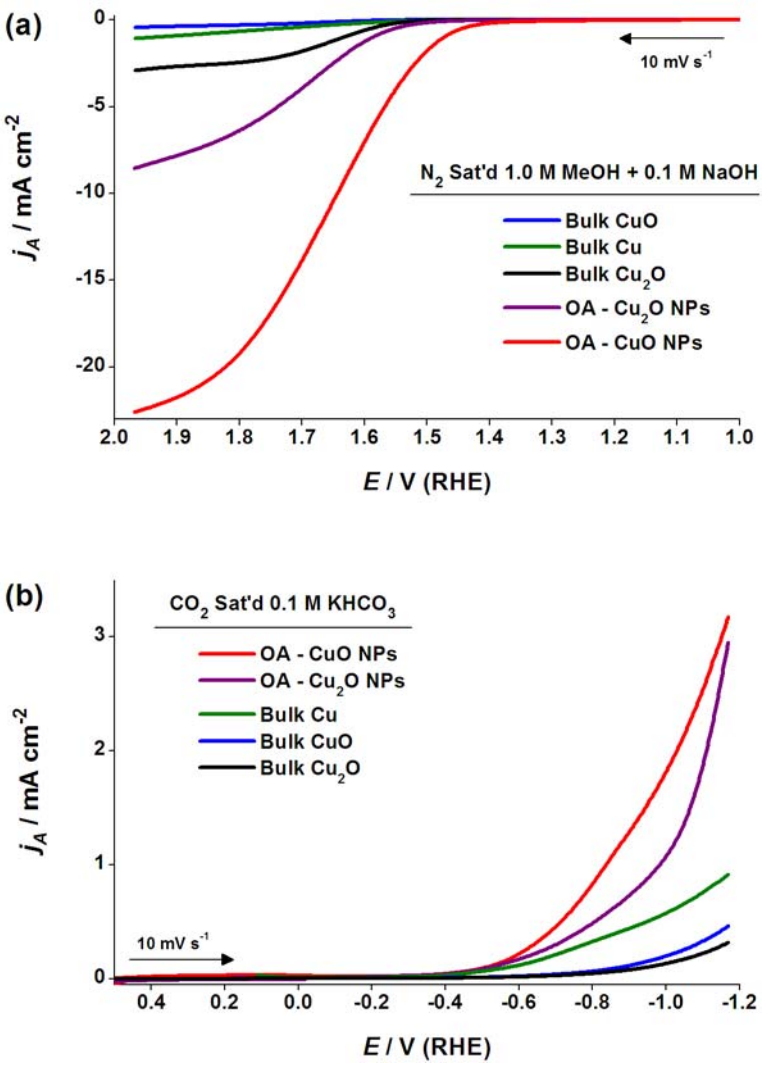

Figure S8. Stabilized (a) MeOH oxidation and (b) CO_2 reduction curves for CB-supported Cu oxides plotted with the current normalized to each catalyst's electrochemical surface area (ECSA), *i.e.* current density, j_A; see experimental section (pages S3–S4) for details on ECSA calculation.

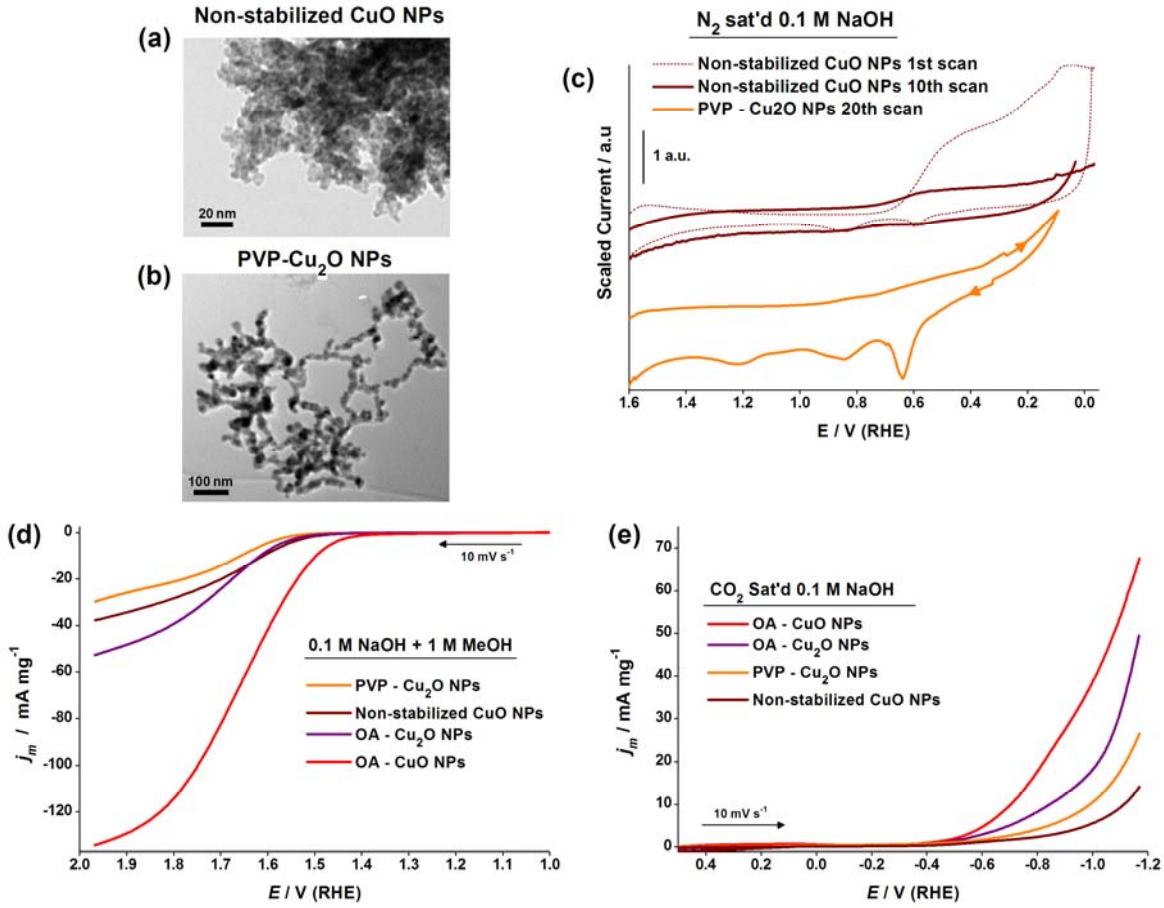

Figure S9. TEM images of (a) non-stabilized CuO NPs and (b) PVP-stabilized Cu_2O NPs. (c) CVs of non-stabilized CuO NPs and PVP-Cu_2O NPs in N_2 saturated 0.1 M NaOH; curves have been offset and a scan rate of 10 mV s^{-1} was used. (d) MeOH oxidation curves of PVP-Cu_2O NPs, non-stabilized CuO NPs and the OA stabilized Cu oxide NPs. (e) CO_2 reduction curves of PVP-Cu_2O NPs, non-stabilized CuO NPs and the OA stabilized Cu oxide NPs.

TEM images (a,b) show non-stabilized CuO NPs (average diameter of 5 ± 2 nm) and PVP-Cu_2O NPs (average diameter of 22 ± 6 nm). In NaOH the PVP-Cu_2O NPs (panel c; orange curve) show a feature characteristic of mixed oxide/hydroxide layer formation similar to that of the bulk Cu oxide catalysts (Fig. S5). This behavior indicates that the weak C=O and C-N coordination bonds that attach PVP to the Cu_2O NP surface[16] are not sufficient to prevent the formation of the mixed oxide/hydroxide layer. On the other hand, the non-ligand stabilized CuO NPs appear to dissolve when cycled through anodic potentials in NaOH (panel c; brown traces). Specifically, the non-ligand CuO NPs eventually lost characteristic redox peaks during CV experiments and we could detect Cu^{n+} ions in solution using a freshly cleaned and polished glassy carbon working electrode.

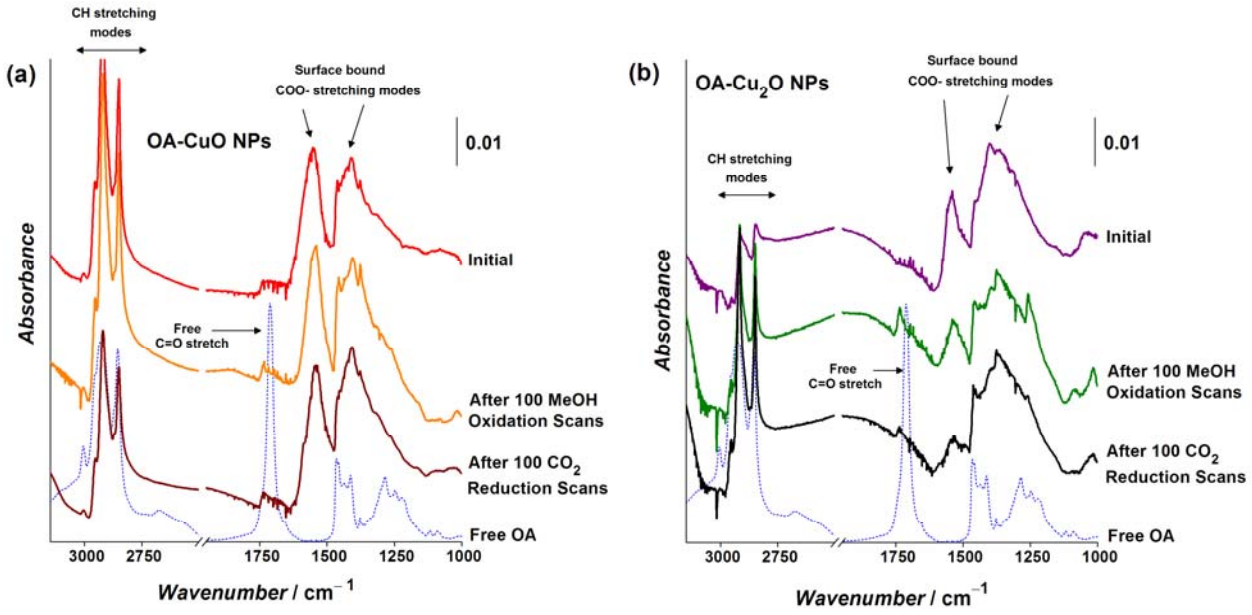

Figure S10. FTIR absorbance spectra of (a) OA-CuO NPs and (b) OA-Cu_2O before and after 100 MeOH oxidation and CO_2 reduction cycles. The plots also contain spectra of free oleic acid (blue dashed curve) to show the difference in peak locations; the spectra have been scaled and offset for comparison.

We find characteristic peaks for surface bound OA after 100 cycles of MeOH oxidation and CO_2 reduction; please see Fig. S3 for details on peak identification. The persistence of these surface bound OA peaks indicates that the ligands remain covalently bound to the NP system during electrocatalytic reactions.

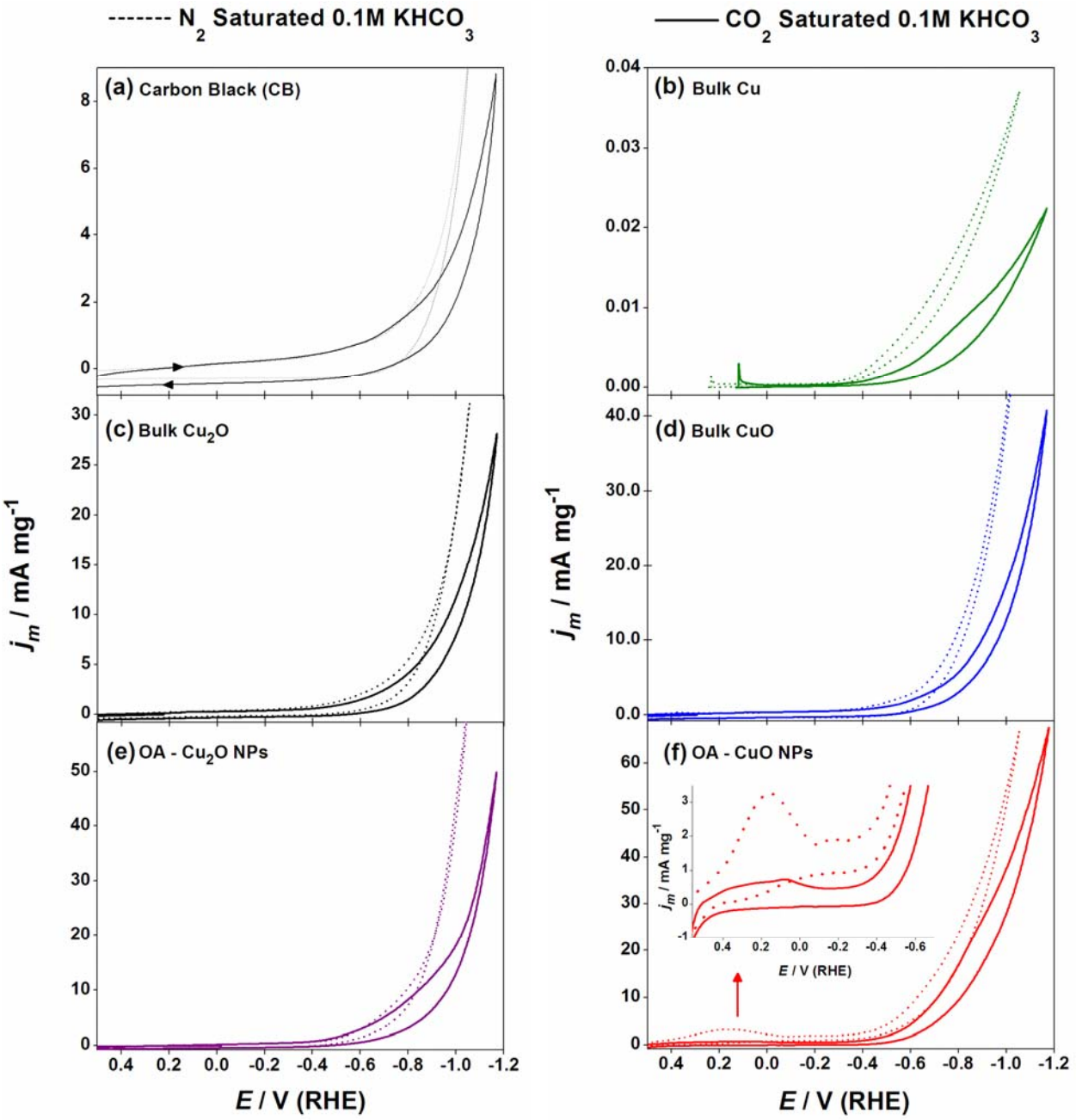

Figure S11. Stabilized CVs of CB-supported Cu oxides in N_2 (dashed curves) and CO_2 (solid curves) saturated 0.1M $KHCO_3$; the scan direction is labeled with arrows in panel a, and the scan rate was 10 mV s^{-1} for all plots. The inset of panel f shows an expanded view of the $Cu^{+/0}$ redox region of the OA-CuO NPs. Decreased mass activity at potentials towards more cathodic potentials in CO_2 saturated solutions is common for Cu-based metals, and it has been attributed to reduced H_2 production due to CO_2 adsorption.[17]

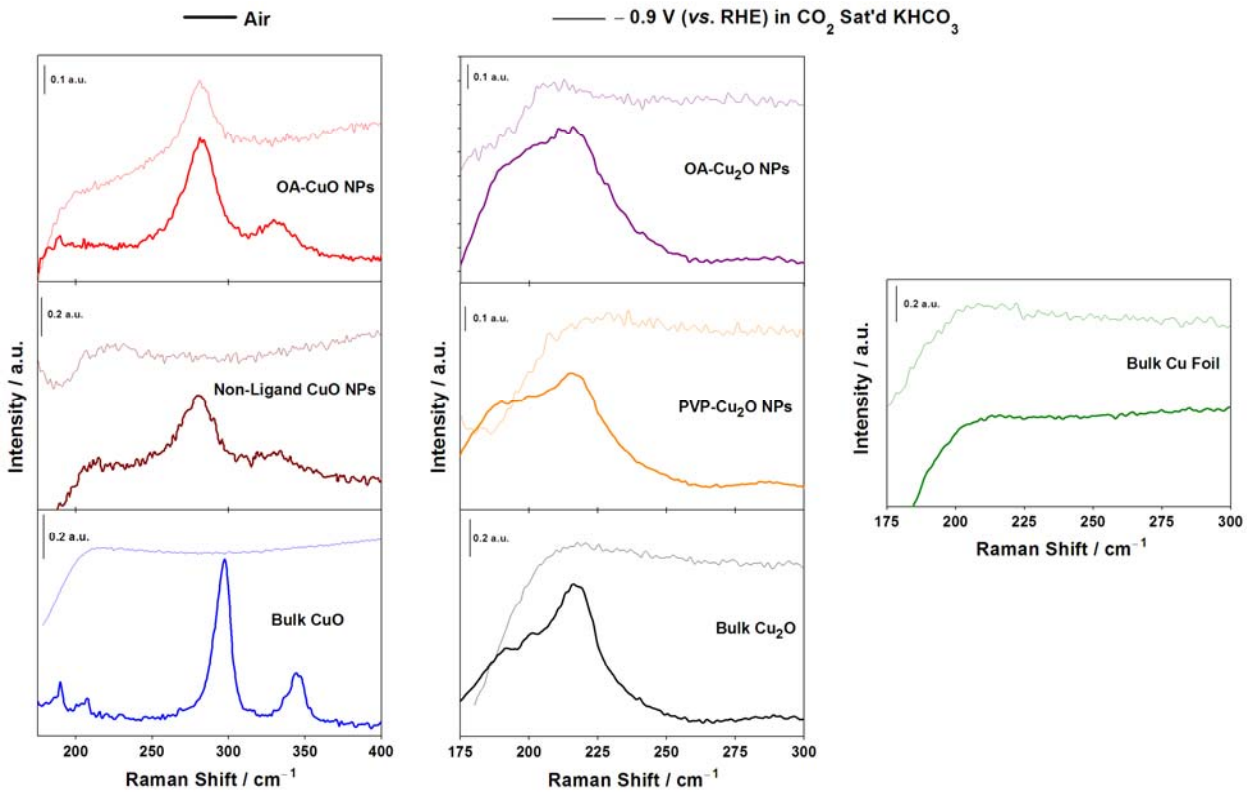

Figure S12. Raman spectra of catalyst materials in air (thick lower curves) and during the application of –0.9 V (*vs.* RHE) in CO_2 saturated 0.1 M $KHCO_3$ (thin upper curves); spectra have been normalized and offset.

The OA-CuO NPs retain an apparent oxide peak during the application of –0.9 V (*vs.* RHE) in CO_2 saturated 0.1 M $KHCO_3$, indicating the OA ligands sustain some fraction of oxide groups on the NP surface despite the cathodic potential. However, during the application of –0.9V the other bulk and nanoparticulate materials develop a sloped and relatively featureless spectrum comparable to that of bulk Cu foil. The OA-Cu_2O NP results are less clear, and we are not able to unambiguously determine if oxide-related peaks are retained during the application of –0.9 V. However, FTIR absorbance spectroscopy indicates retention of OA ligands after CO_2 reduction reactions (Fig. S10), indicating retention of some fraction of covalent O-Cu bonds at the NP surface.

Table S1. MeOH oxidation and CO_2 reduction product distributions for the Cu oxide catalysts.

MeOH Oxidation

	HCOH (mmol g^{-1} hr^{-1})	CO_2 (mmol g^{-1} hr^{-1})	Average run-to-run HCOH Selectivity (%)	Average run-to-run CO_2 Selectivity (%)
Oleic Acid CuO NPs	781.9 ± 148.9	0.25 ± 0.067	99.968 ± 0.003	0.032 ± 0.003
Bulk CuO*	< 0.15	1.210 ± 0.004	< 11	> 89
Oleic Acid Cu_2O NPs	221.4 ± 100.4	30.84± 0.30	88 ± 7	12 ± 7
Bulk Cu_2O*	< 0.15	0.880 ± 0.003	< 14.6	> 85.4
PVP-Cu_2O NPs*	< 0.15	7.55 ± 0.24	< 1.9	> 98.1
Non-stabilized CuO NPs*	< 0.15	2.19 ± 0.57	< 6.4	> 93.6

* HCOH was not present above the detection limit, which equals 0.15 mmol g^{-1} hr^{-1} for the Cu oxide samples.

CO_2 Reduction

	CO (mmol g^{-1} hr^{-1})	H_2 (mmol g^{-1} hr^{-1})	Average run-to-run CO/H_2 Ratio	Average run-to-run CO Selectivity (%)	Average run-to-run H_2 Selectivity (%)
Oleic Acid CuO NPs	7.18773 ± 0.307773	4.62333 ± 0.16258	1.55 ± 0.07	61 ± 3	39 ± 3
Bulk CuO	1.01733 ± 0.19375	1.165 ± 0.30406	0.9 ± 0.1	47 ± 9	53 ± 9
Oleic Acid Cu_2O NPs	3.46167 ± 0.17718	6.55667 ± 0.330807	0.53 ± 0.03	35 ± 2	65 ± 2
Bulk Cu_2O	1.022333 ± 0.25739	4.62333 ± 0.16258	0.32 ± 0.06	21 ± 4	79 ± 4
PVP-Cu_2O NPs	0.2550 ± 0.13717	3.65667 ± 0.15275	0.07 ± 0.04	7 ± 4	93 ± 4
Non-stabilized CuO NPs	0.727333 ± 0.130631	2.99 ± 1.19503	0.17 ± 0.06	20 ± 7	80 ± 7

HCOOH was not present above the detection limit, which equals 11.6 mmol g^{-1} hr^{-1} for the Cu oxide samples.

Supporting Information References

(1) Yin, M.; Wu, C. –K.; Lou, Y.; Burda, C.; Koberstein, J. T.; Zhu, Y.; O'Brien, S. Copper Oxide Nanocrystals. *J. Am. Chem. Soc.* **2005**, *127*, 9506-9511.

(2) Zhu, J.; Li, D.; Chen, H.; Yang, X.; Lu, L.; Wang, X. Highly Dispersed CuO Nanoparticles Prepared by a Novel Quick-Precipitation Method. *Mater. Lett.* **2004**, *58*, 3324-3327.

(3) Shaak, R. E.; Sra, A. K.; Leonard, B. M.; Cable, R. E.; Bauer, J. C.; Han, Y. –F.; Means, J.; Teizer, W.; Vasquez, Y.; Funck, E. S. Metallurgy in a Beaker: Nanoparticle Toolkit for the Rapid Low-Temperature Solution Synthesis of Functional Multimetallic Solid-State Materials. *J. Am. Chem. Soc.* **2005**, *127*, 3506-3515.

(4) Bard, A. J.; Faulkner, L. R. *Electrochemical Methods: Fundamentals and Applications, 2nd Edition*; John Wiley & Sons: New York, 2001.

(5) Trasatti, S.; Petrii, O. A. Real Surface Area Measurements in Electrochemistry. *Pure & Appl. Chem.* **1991**, *63*, 711-734.

(6) Waszczuk, P.; Zelenay, P.; Sobkowski, J. Surface Interaction of Benzoic Acid with Copper Electrode. *Electrochim. Acta* **1995**, *40*, 1717-1721.

(7) Chou, M. H.; Liu, S. B.; Huang, C. Y.; Wu, S. Y.; Cheng, C. –L. Confocal Raman Spectroscopic Mapping Studies on Single CuO Nanowire. *Appl. Surf. Sci.* **2008**, *254*, 7539-7543.

(8) a) Richter, H.; Wang, Z. P.; Ley, L. The One Phonon Raman Spectrum in Microcrystalline Silicon. *Solid State Comm.* **1981**, *39*, 625-629. b) Zi, J.; Büscher, H.; Falter, C.; Ludwig, W.; Zhang, K.; Xie, X. Raman Shifts in Si Nanocrystals. *Appl. Phys. Lett.* **1996**, *69*, 200 (3 pages).

(9) Dawson, P.; Hargreave, M. M.; Wilkinson, G. R. The Dielectric and Lattice Vibrational Spectrum of Cuprous Oxide. *J. Phys. Chem. Solids* **1973**, *34*, 2201-2208.

(10) a) Wu, C. –K.; Yin, M.; O'Brien, S.; Koberstein, J. T.; Quantitative Analysis of Copper Oxide Nanoparticle Composition and Structure by X-ray Photoelectron Spectroscopy. *Chem. Mater*. **2006**, *18*, 6054-6058. b) Chusuei, C. C.; Brookshier, M. A.; Goodman, D. W. Correlation of Relative X-ray Photoelectron Shake-up Intensity with CuO Particle Size. *Langmuir* **1999**, *15*, 2806-2808.

(11) Wagner, C. D.; Riggs, W. M.; Davis, L. E.; Moulder, J. F.; Mullenberg, G. E. (Eds.) *Handbook of X-Ray Photoelectron Spectroscopy*; Perkin-Elmer Corp.: Eden Prairie, MN, 1979.

(12) Balamurugan, B.; Mehta, B. R.; Shivaprasad, S. M. Surface-Modified CuO Layer in Size Stabilized Single-Phase Cu_2O Nanoparticles. *Appl. Phys. Lett.* **2001**, *79*, 3176 (3 pages).

(13) a) Wu, N.; Fu, L.; Su, M.; Aslam, M.; Wong, K. C.; Dravid, V. P. Interaction of Fatty Acid Monolayers with Cobalt Nanoparticles. *Nano Lett.* **2004**, *4*, 383-386. b) Simon-Kutscher, J.; Gericke, A.; Hühnerfuss, H. Effect of Bivalent Ba, Cu, Ni, and Zn Cations on the Structure of Octadecanoic Acid Monolayers at the Air−Water Interface As Determined by External Infrared Reflection−Absorption Spectroscopy. *Langmuir* **1996**, *12*, 1027-1034.

(14) Liu, X.; Geng, B.; Du, Q.; Ma, J.; Liu, X. Temperature-Controlled Self-Assembled Synthesis of CuO, Cu_2O and Cu Nanoparticles Through a Single-Precursor Route. *Mater. Sci. Eng. A* **2007**, *448*, 7-14.

(15) a) Strehblow, H. –H.; Titze, B. The Investigation of the Passive Behavior of Copper in Weakly Acidic and Alkaline Solutions and the Examination of the Passive Film by ESCA and ISS. *Electrochim. Acta* **1980**, *25*, 839-850. b) Brisard, G. M.; Rudnicki, J. D.; McLarnon, F.; Cairns, E. J. Application of Probe Bean Deflection to the Study the Electrooxidation of Copper in Alkaline Media. *Electrochim. Acta* **1995**, *40*, 859-865. c) Abd el Haleem, S. M.; Ateya, B. G. Cyclic Voltammetry of Copper in Sodium Hydroxide Solutions. *J. Electroanal. Chem.* **1981**, *117*, 309-319.

(16) a) Haas, I.; Shanmugam, S.; Gedanken, A. Pulsed Sonochemical Synthesis of Size-Controlled Copper Nanoparticles Stabilized by Poly(N-vinylpyrrolidone). *J. Phys. Chem. B* **2006**, *110*, 16947-16952. b) Zhang, Z.; Zhao, B.; Hu, L. PVP Protective Mechanism of Ultrafine Silver Powder Synthesized by Chemical Reduction Processes. *J. Solid State Chem.* **1996**, *121*, 105-110.

(17) a) Hori, Y.; Murata, A.; Takahashi, R. Formation of Hydrocarbons in the Electrochemical Reduction of Carbon Dioxide at a Copper Electrode in Aqueous Solution. *J. Chem. Soc. Faraday Trans. 1* **1989**, *85*, 2309-2326. b) Takahashi, I.; Koga, O.; Hoshi, N.; Hori, Y. Electrochemical Reduction of CO_2 at Copper Single Crystal Cu(S)-[*n*(111) × (111)] and Cu(S)-[*n*(110) × (100)] Electrodes. *J. Electroanal. Chem.* **2002**, *533*, 135-143. c) Hori, Y. Electrochemical CO_2 Reduction on Metal Electrodes. *Modern Aspects of Electrochemistry*; Vayenas, C. G.; White, R. E.; Gamboa-Aldeco, M. E.; Eds. Springer, New York, **2008**, *42*, 89-189. d) Gattrell, M.; Gupta, N.; Co, A. A Review of the Aqueous Reduction of CO_2 to Hydrocarbons at Copper. *J. Electroanal. Chem.* **2006**, *594*, 1-19.